Atmospheric Research 202 (2018) 175–186

Contents lists available at ScienceDirect

Atmospheric Research

journal homepage: www.elsevier.com/locate/atmosres

Exploring radar and lightning variables associated with the Lightning Jump. Can we predict the size of the hail?

C. Farnell*, T. Rigo, N. Pineda

Meteorological Service of Catalonia, C/Berlin, 38-46, Barcelona, Spain

ARTICLE INFO

Keywords:
Lightning Jump
Hail size
Catalonia
Radar variables
Nowcasting

ABSTRACT

Severe weather regularly hits the Lleida Plain (western part of Catalonia, NE of Iberian Peninsula), causing important damage to the local agriculture. In order to help severe weather surveillance tasks, the Meteorological Service of Catalonia (SMC) implemented in 2016 the Lightning Jump (LJ) algorithm as operative warning tool after an exhaustive validation phase of several months. The present study delves into the analysis of the relationship between Lightning Jump alerts and hail occurrence, through the analysis of lightning and radar variables in the moment when the warning is issued. Overall, the study has consisted of the analysis of 149 cases, grouping them into two categories according to hail size: small and large hail, with a threshold of 2 cm of diameter. The thunderstorms related to big sized hail presented remarkable differences in some of the variables analysed that could help forecast the size of hail when the LJ alert is triggered. Moreover, other variables have been allowed to observe and to corroborate how the LJ algorithm works during the 13 min before the warning is triggered.

1. Introduction

Hailstorms produce important damage and economic losses. Consequently, they are widely studied in different latitudes and climates. Some examples are Mendoza, Argentina (Makitov, 1999), Alberta, Canada (Krauss and Marwitz, 1984; Krauss and Renick, 1997), Colorado, USA (Browning and Foote, 1976), Finland (Tuovinen et al., 2009), Caucasus, Russia (Makitov et al., 2016), or the Ebro Valley, Spain (Castro et al., 1992). Most of the hail episodes in Europe occur during the warm season (e.g. Dessens, 1986; Giaiotti et al., 2003; Sánchez et al., 1996), in areas close to or influenced by mountain ranges, which contribute to the triggering or enhancement of convection (Makitov et al., 2016). In economic terms, Punge and Kunz (2016) reported that losses during 2014 exceeded € 1 B only in Central Europe.

Focusing on the Lleida Plain, our region of study, the hailstorm season takes place from April to September (Rigo and Llasat, 2016). The hail events are more frequent in April and May, but the largest diameters usually occur in July and August. According to this, as the season goes on, the frequency of events decreases, but their severity increases. Since these months encompass the most vulnerable phase of the vegetative cycle of the orchards in the region (e.g. apples, pears, peaches), hail damage causes high economic losses. In this sense, Aran et al. (2011) estimated that, between 2000 and 2009, the economic losses in crops across the Lleida plain were of € 15 M.

According to Schultz et al. (2014), the hailstorms result from deep convection, which generally presents intense lightning activity. Moreover, the predominant flash types (intra-cloud, hereafter IC, or cloud-to-ground, CG, which can be positive or negative) may change, depending on the phase of the thunderstorm's life cycle (MacGorman et al., 1989). Moreover, the predominance of a particular type of flashes (e.g. Goodman et al., 2005; Metzger, 2010; Yao et al., 2013) can be related to the different forms of severe weather that may take place (severe weather is defined as the presence of large hail, straight convective winds and/or tornados). In this sense, high values of the IC/CG ratio have been related to severe thunderstorms (e.g. Carey and Rutledge, 1998; Montanyà et al., 2007). Besides this, Lang et al. (2000) reported that the initial production of hail at high levels corresponds to a rapid increase of the IC/CG ratio. Along the same lines, MacGorman et al. (1989) observed that the strong updrafts present in severe thunderstorms could lift the negative charge to higher altitudes within the cloud, favouring ICs in detriment of CG flashes. Considering only the latter type of flashes, some positive anomalies have been observed during the mature phase of the severe thunderstorm in particular cases of study (e.g. Montanyà et al., 2009; Pineda et al., 2016). To complete the analysis of the life cycle of severe thunderstorms, Williams et al. (1989) found that the lightning activity starts with IC flashes exclusively, just after the development of the icing phase in the cloud. Furthermore, after the occurrence of the first IC peak, a maximum of CG

* Corresponding author.
E-mail address: cfarnell@meteo.cat (C. Farnell).

https://doi.org/10.1016/j.atmosres.2017.11.019
Received 7 June 2017; Received in revised form 10 November 2017; Accepted 12 November 2017
Available online 14 November 2017

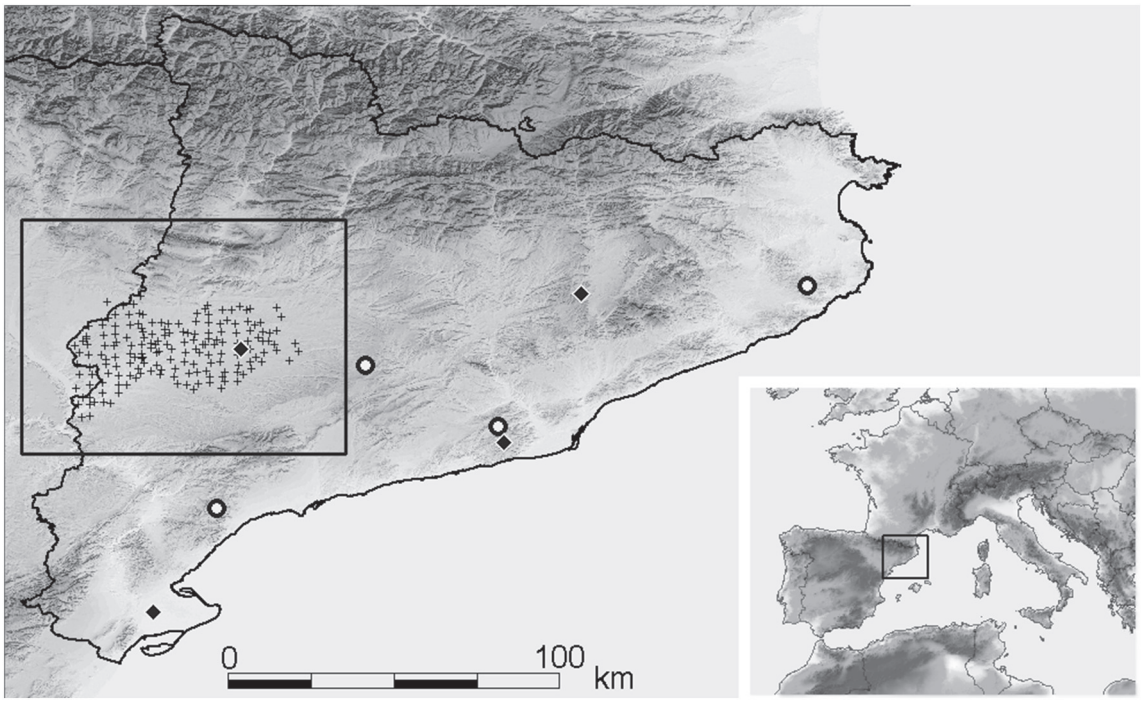

Fig. 1. Map of the area of study: Catalonia within western Europe (bottom right) and the Lleida Plain in Catalonia (left). The different data sources used are displayed: Hailpad network (crosses), weather radar network (dots) and lightning station locations (diamonds).

may be recorded, according to Soula et al. (2004) and Carey and Rutledge (1998). Then, positive CG flashes could be dominant during the mature phase of severe weather, with respect to the total CG rate. However, Pineda et al. (2016) observed an erratic behaviour of CG lightning in front of clear patterns of IC lightning. In any case, several studies have reported a sudden increase of the Total Lightning (hereafter, TL) ratio some minutes before the occurrence of severe weather (Goodman et al., 1988; Lang et al., 2000; MacGorman et al., 1989; Williams et al., 1999, 1989). By definition, TL is the sum of IC and CG flashes. Lightning Jump (hereafter LJ) is the sudden increase of TL. Several algorithms have been developed for identification of the LJ, with the purpose of using it as a severe weather forecast tool (Gatlin and Goodman, 2010; Goodman et al., 2005; Schultz et al., 2009).

For the evaluation of the LJ algorithm, the Lead Time (hereafter LT) measures the time between the triggering of the warning provided by the tool and the occurrence of severe weather at the surface. According to different authors, the LT is variable, depending on the type of thunderstorm. For instance, Williams et al. (1999) found a LT between 5 and 20 min in thunderstorms with microbursts, while Steiger et al. (2007) determined a LT around of 5–30 min in an analysis of supercells. Finally, Metzger (2010) calculated an average LT of 14 min in the analysis of 18 cases of severe weather. One of the main problems when calculating the LT is the absence of ground observations. In these cases, a hailstorm can go unnoticed or underestimated(Smith et al., 2012; Trapp et al., 2006). Then, the lack of hail observations at surface requires that other methods or products are considered in order to estimate the magnitude of the phenomenon and the affected area. In this regard, weather radar observations can be used to detect the presence of hail and to estimate the affected area (e.g. Bringi et al., 1986; Farnell et al., 2016; Witt et al., 1998). VIL (Vertically Integrated Liquid) is one of the radar products used for detecting hail within the cloud. A high value of VIL generally indicates a high content of water or ice in the thunderstorm (Boudevillain and Andrieu, 2003; Edwards and Thompson, 1998). Moreover, a sudden increase of the VIL means that the thunderstorm is gaining intensity and that the presence of hail becomes possible. Therefore, VIL is directly linked with the updraft speed and with the cloud depth (Kitzmiller et al., 1995). Furthermore, it can be related to the height where lightning begins (Steiger et al., 2007).

The present paper further develops the research started by Farnell et al. (2017) (hereafter, F2017), which studied the performance of the LJ algorithm in 59 episodes of severe weather in Catalonia. F2017 showed that LJ tool had forecast 75% of the events and, while producing only 10% of false alarms. Hence, the aim of this paper is to determine if it is possible to make a prediction of the maximum hail size, just in the moment when the LJ algorithm triggers an alert. To this end, diverse characteristics related to the LJ in hail-bearing thunderstorms are analysed. The manuscript contains the following sections. Initially, the paper introduces the area of study. The next section describes the data and methodology used. After these sections, the presentation of the results includes seven subsections. The first subsection is a preliminary analysis of hail events in the affected region. The second subsection studies how the area and the TL evolve during the 13 min before the LJ warning. The third subsection analyses the predominance of the different types of flashes. The fourth subsection evaluates the behaviour of IC, +CG and −CG flashes. The fifth subsection describes the validation of the LJ tool by means of the LT and the distance between region where the alert was issued and the region where severe weather was observed. The last two subsections consist of the analysis of the vertical profile of radar reflectivity and of the convective mode of those thunderstorms most prone to produce the LJ alerts. The discussion of the results in the following section presents a comparison of the results with other works. This leads to the final section, the conclusions.

2. Area of study

This study is centred in the Lleida Plain (Fig. 1), a region bounded by the meridians 0.3° E and 1.5° E and the parallels 41.2° N and 42.2° N, located at the Midwest part of Catalonia (at the NE of the Iberian Peninsula). It is a region of approximately 5600km^2, with terrain elevations ranging between 200 and 400 m. Three mountain ranges limit the region, at the North, the East, and the South (with altitudes between 800 and 1600 m). Moreover, the plain merges with the Ebro Valley depression to the West.

As mentioned above, agriculture is one of the most important economic activities of the region. For this reason, several studies have focused on hail events that have affected this area (e.g. Aran and Pena, 2009; Aran et al., 2011; Farnell et al., 2009; Pascual, 2002; Rigo and Pineda, 2016)).

3. Data and methodology

3.1. Data

The different types of data used in this work go from surface observations to remote sensing data.

3.2. Hailpads

The network of hailpads is composed of 170 elements (Fig. 1), distributed in an approximately regular mesh of $\sim 4 \times 4\ km^2$. The Associació de Defensa Vegetal (ADV, Association for Plant Protection) deployed the network back in 1990, in order to have a better knowledge of the hailstorms that affect the Lleida plain. Currently, the ADV collects the plates after each event with the purpose of providing a first estimation of the hail effect. The Group of Physics of the Atmosphere of the University of Leon analyses each hailpad immediately after the hail campaign finishes. The process starts every year approximately at the end of October and lasts for some months, depending on the number of affected pads. When this process concludes, several hail variables such as maximum diameter, number of impacts, or their kinetic energy are available for each of the events that occurred in the region (Palencia et al., 2007).

Dalezios et al. (2002) casted doubt on the ability to detect the maximum diameter of a hail event by means of a hailpad network with a density such as the one used in the present analysis. Addressing this issue, Farnell et al. (2016) showed that the combination of hailpad observations with radar fields usually provides good hail size estimation maps, applying the Universal Cokriging technique.

The hail observations of the ADV network have allowed the analysis of the variability of the events throughout the studied period. Moreover, these registers and the thunderstorm paths have been combined for calculation of the maximum hail size measured at surface for each of the convective cells that triggered any LJ alert during the life cycle.

3.3. XDDE: Lightning Location System (LLS)

The Meteorological Service of Catalonia (SMC) operates a LLS (here cited as SMCLLS), that was installed in 2003. The SMCLLS combines the detection of cloud-to-ground (CG) and intra-cloud (IC) flashes, using sensors of Low Frequency (LF) and of Very High Frequency (VHF), respectively. The SMCLLS is composed of four detectors (Fig. 1), strategically located in order to obtain a good coverage over all the territory of Catalonia. Throughout the years of operation, the SMCLLS performance has been experimentally evaluated in successive campaigns by means of electromagnetic field measurements and video recordings of natural lightning (Montanyà et al., 2006, 2012; Pineda and Montanyà, 2009). Results from those campaigns have established, for the SMCLLS, a CG flash Detection Efficiency of around $80-85\%$ and location accuracy below 1 km.

In the present study, the lightning data has been applied twofold. First, it has been used for the retroactive triggering of warnings, applying from the LJ algorithm to the 2006–2013 period, as described in F2017 (see upcoming Subsection 3.5). The second use of the SMCLLS data has been the analysis of the CG and IC flashes during the 13 min prior to each of the LJ warnings previously identified.

3.4. XRAD: Radar Network

The Radar Network (XRAD, from the Xarxa de Radars de Catalunya) of the SMC is composed of 4 C-band Doppler weather radars (Fig. 1), operating in single polarization. The SMC developed the XRAD to provide quantitative precipitation estimations (QPE) with high resolution, among other products of interest for meteorological and hydrological purposes (Rigo et al., 2010; Trapero et al., 2009). Composite imagery of the XRAD allows to mitigate the negative effects that can affect single radar volumes (e.g. signal attenuation, or signal blockage). The spatial distribution of the XRAD is such that it covers the 96% of the Catalan territory. Moreover, the overlapped scan of two or more radars covers the 58% of the Catalan area. One of the most challenging aspects related to radar information is the difficulty for identifying patterns associated with severe weather, given the complexity of the shapes in radar imagery (Doswell III, 2001; Heinselman et al., 2008; Przybylinski, 1995). Therefore, the combination of radar imagery with lightning is advantageous for improving the nowcasting of severe weather events.

The use of weather radar data in this work has two purposes. Firstly, the reflectivity fields have allowed the identification of the path of the thunderstorm that had produced the LJ warning in each event. This point is very important in events with several thunderstorms affecting the area of study, because it allows to discriminate which one was the warning triggerer. Secondly, different radar products have helped to determine the characteristics of the thunderstorm at the time at which the LJ algorithm issued the warning, helping to understand the internal mechanisms of the thunderstorm at that time.

3.5. Methodology

F2017 studied the application of the LJ algorithm as a forecast tool of severe weather in Catalonia. The LJ algorithm used departs from the Schultz et al. (2009) methodology; some modifications with respect to the original routine have been implemented, in order to adapt it to the conditions of the area of study. The main difference between the two algorithms is the technique for identification of the thunderstorms. While the old version detected the convective cells using radar data, the adaptation (F2017) identifies the structures using exclusively total lightning data. The new detection technique consists of the following points: (i) Each minute, a query to the lightning database provides the current time and a file with the flashes detected during the previous 13 min(this time period is the same as in the original method). (ii) If any IC or CG flashes are detected, the procedure progresses to the next steps (otherwise, the process stops). (iii) A rasterization (that is, a conversion of points to a raster -or geo-referenced matrix-) of the lightning flashes is applied with a spatial resolution of $1 \times 1\ km^2$. This step also differs from the original technique, which all the time considers flashes as points. The resulting raster represents the number of lightning flashes within each pixel. Afterwards, contiguous pixels with more than one flash are grouped into structures, applying a neighbouring technique (see for instance, Rigo et al., 2010). (iv) Once the algorithm detects a flash structure in the current time, the process is applied for the whole 13 min period (the period of analysis). If the structure has maintained a continuity of flash activity in time and space during the period, the tool evaluates the cell, with the purpose of determining if a sudden increase of the activity has been registered during the last minute. (v) The last point consists of issuing a warning (Lightning Jump warning, hereafter LJW) if during the current minute the number of flashes has exceeded two times the standard deviation for the complete period. The LJW position is defined as the location of the centroid of the cell at minute 14.

The present study analyses 149 cases from the 2006–2013 period. Each case corresponds to a convective structure for which the following two premises are fulfilled: hail has been recorded in at least one hailpad, at least one LJW has been registered during its life cycle.

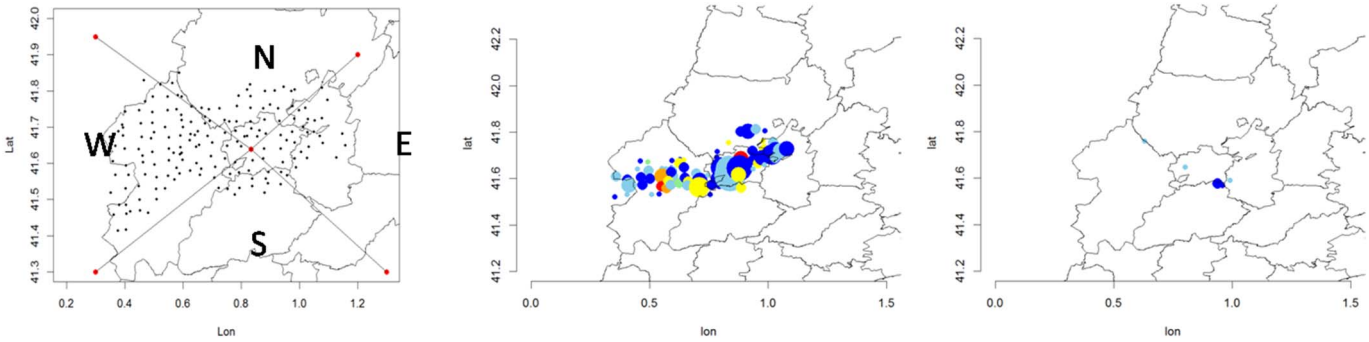

Fig. 2. Left) separation of the study area in four quadrants (northern, southern, western, eastern); centre) example of an extensive episode (more than 11 hailpads affected); right) example of a local hail episode (less than 11 hailpads affected). Longitude and latitude units are in degrees.

During the period analysed, 231 LJW have been issued, and 218 of them have been related to hail episodes. Radar data was not available for the 17 remaining LJ warnings. From those 214 LJ alerts, 149 have associated with hail episodes that affected the area of study, while the other 65 LJW correspond to hail episodes that did not affect the hailpads area (hence, hail diameter is not available). The episodes are classified in two categories according to the maximum hail size registered: 72 cases recorded hail below 2 cm (hereafter G1), while 77 cases registered hail equal or over 2 cm (G2).

In order to characterize the set of hailstorms, the extension and location of the hailswath has been studied (Fig. 2). To analyse the area affected by the thunderstorms, which can be local or extensive, the total number of hailpads affected in each episode has been considered. In this sense, the threshold between local and extensive cases has been calculated using the quantile 75 for the whole set of cases. It has been observed that this threshold was 11. In order to determine analysing the zone most affected by hailstorms, the hailpad region has been divided into four quadrants (N, S, E, W), identifying in which quadrant the percentage of hailpads affected is higher.

The method for evaluation of the LJ algorithm consists of the following steps:

Step 1. The maximum diameter of hail registered in the hailpads is associated with the cell that has produced the LJW, with the goal of classifying its severity. Then, four procedures are carried out (Fig. 3) for each thunderstorm.
1.1) The date and hour for each LJW is determined, running the algorithm over the lightning flashes database for the period of study. 1.2) The plot of the radar-estimated accumulated precipitation for the period that goes from 3 h before to 3 h after the time of the LJW record allows to discriminate the paths of the different thunderstorms observed during the period. 1.3) The structure of the precipitation associated with the location of the LJW is extracted. 1.4) The maximum hail diameter registered by hailpads is selected, considering the connection between surface observations and the precipitating system extracted in the previous stage 1.3.
Step 2. The lightning records during the 13-min period preceding the LJW time are considered. The evolution of these is analysed in order to know the behaviour during the study period.
Step 3. The data normalization technique used in Rigo et al. (2010) is applied with the purpose of easily comparing the behaviour of the electrical activity between the different episodes and groups. Briefly, the technique consists of normalizing all the variables individually with respect to the maximum value during the whole period. The following percentiles are calculated for all episodes and for all normalized variables: 1 (hereafter P1), 25 (P25), 50 (P50), 75 (P75), and 99 (P99).
Step 4. The 13 min before the time of the LJW is analysed. The last 2 min is discarded because it is when the increase of lightning occurs by definition. This study has the aim of identifying possible common

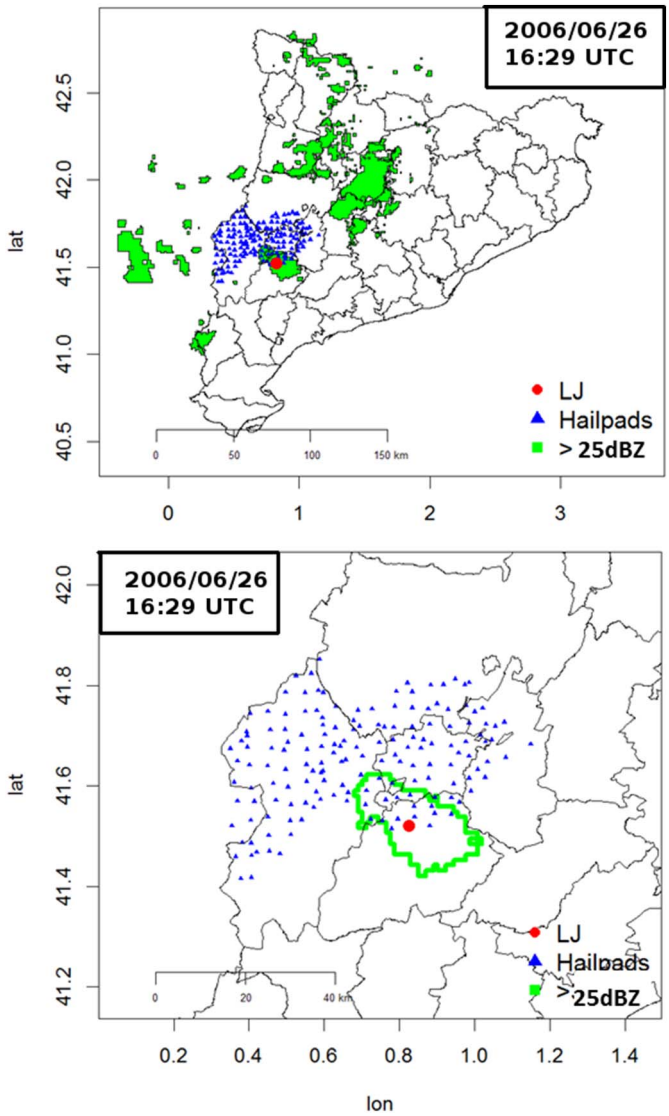

Fig. 3. Relationship between structures of precipitation and hailpads. The green colour corresponds to areas with reflectivity > 25 dBZ, the blue points are the hailpads and the red point is a LJW. Longitude and latitude units are in degrees.

patterns in the behaviour of thunderstorms just before the alert. The analysis is carried on considering TL, Area (number of pixels with TL observations), IC, +CG and −CG flash for each episode and group. Each variable may be characterized by three possible trends: positive, negative and neutral. To define the trend, their evolution during the 10 min period is minute-by-minute studied. Values < 2

are characterised as a negative trend, > 2 as a positive trend, and the rest as a neutral trend.

Step 5. The distance between the LJ alert position and the location of severe weather is calculated for each case, taking into account the maximum hail-sizes obtained by hailpads. However, the lead time calculation is more complicated. Since the hailpads do not record the time of the observations, the time of the maximum hail register is estimated from the time when the maximum value of VIL over the hailpad is recorded. The results are plotted using box plots, based on quartiles. The sample is divided in 5 parts: minimum, Q1 (P25), Q2 (median), Q3 (P75) and the maximum. The interquartile range is the sample fraction that lies between Q1 and Q3. These statistics give valuable information about the differences in time and position between warnings and observations.

Step 6. A volumetric analysis of radar data is carried on the vertical profile over the point where the LJW occurred, in order to determine the vertical development of the radar structures (only the pixels located within a 10 km radius around the LJ alert zone were considered). The CAPPI radar product used in the analysis is a composition of the individual volumes of all the radars of the XRAD. It covers the whole territory of Catalonia and its part of its neighbouring areas. It has a horizontal resolution of $2 \times 2\ km^2$, a vertical one of 1 km, with levels from 1 to 10 km, and a time resolution of 6 min. The resulting product is an indicator of the vertical profile of reflectivity of thunderstorms during the LJW.

Step 7. The radar structures associated with the LJW are categorised. The set of thunderstorms is divided into seven modes, according to the reflectivity field at the surface: 1) Isolated cell (ISO), defined as a small region of high reflectivity values, and surrounded by areas without reflectivity. 2) Like-Supercell (SPC), which is similar to the previous one, but larger, with shapes that may be associated with rotation, such as a hook echo. 3) Multicell (MUL), a cluster of reflectivity cells with an unclear organization. 4) Squall Line (SQL), defined as a multicell, but linearly organized. 5) Mesoscalar Convective System (MCS), similar to squall lines, but with an axis exceeding 100 km. 6) Bow Echo (BOW), defined as a squall line structure, arched in the central part of the axis. 7) NA, for those cases that are far from the radar and the structure is not clearly identifiable. This classification is based on Rigo and Llasat (2004), Fraile et al. (2001) and Smith et al. (2012). Fig. 4 shows examples of each structure. The classification is made in a visual way for each case. This step determines which convective modes are more associated with LJW.

4. Results

The upcoming analysis focuses on the relationship between hail at the surface and the LJW, on the evolution of the different variables associated with the lightning activity, and, finally, on the patterns of radar reflectivity of the thunderstorms. The purpose of the analysis is to find those characteristic behaviours that could be key factors when forecasting the hail size, in the moment when the tool activates the LJW.

4.1. Preliminary analysis of hail events (2006–2013)

In order to understand the surface features of hailstorms associated with LJW, the preliminary analysis has considered selected features of the hail observations at the surface. The first analysis focuses on the total number of pads hit during each event. In this sense, the hailstorms have affected the area only locally (that is, less than 11 hailpads) for 74% of the cases. This result cannot be associated with the size of the thunderstorms because some of them affect only partially the area of analysis.

Fig. 2 (left panel) shows the characterization considering quadrants (western, eastern, northern, and southern). The western quadrant presented the highest number of hailstorms (54% of the cases) that produced at least one warning of LJ and hit at least one pad. In a 19% and 16% of cases, the thunderstorms hit at least one hailpad of northern and eastern regions, respectively. Finally, in fewer cases, 11%, the thunderstorms affected the southern area. This distribution indicates two facts: most hailstorms affecting the ADV region came from the Ebro Valley; and hail-producing thunderstorms can reach the area from any cardinal point.

To conclude this section, the total number of LJW, the LJ alerts related to hailstorms, and the number of hail episodes per year in the ADV region have been compared (see Fig. 5). Two types of patterns can be observed: some years present LJW only associated with hail in the ADV (2007, 2008, 2009, 2011 and 2012), while the rest show a high number of LJW not associated with hail in the ADV region. This indicates that for particular years the events have been predominantly focused on the region of study, while for the rest of the years events have been more general. Moreover, for most of the years, the number of LJW associated with hail has been higher than the number of hail episodes. Therefore, more than one LJW per episode is usual in Catalonia.

4.2. Evolution of lightning and area variables

The patterns of TL and area have been analysed with the goal of studying the behaviour during the 13 min before the LJW. With respect to the evolution of TL, the two groups have a similar behaviour (Fig. 6) in terms of the interquartile area, with the area remaining constant during the first 10 min, followed by a slight decrease in the minute 11. From this moment, a high increase takes place, between minute 12 and 13 (near 20% in all groups). Indeed, the final increment is associated with the LJW.

Regarding the area evolution (Fig. 7), the behaviour is similar to the TL's one. The area practically remains constant until minute 11 when a small decrease occurs. Later, in minute 12, the area suffers a sudden increase. The evolution of the area between groups is similar. However, the values for G2 are lower than for G1 during the first 10 min of the period.

Although the analysis is focused on the normalized values, it is important to take into account that high values of TL per minute are necessary so that a cell accomplishes the requirements of continuity in time and space for the lightning activity. In this regard, these rates reach 230 TL/min in the case of G2 and 150 TL/min for G1.

4.3. Predominance of a type of flashes

The analysis of the predominance of the different lightning types allows to find some key features during the 13 min period that precedes the LJW. The analysis has been made including some indicators of severe weather found in the literature and presented in the introduction, like the IC/CG and $+CG/-CG$ ratios (the last one, associated to positive anomalies of CGs).

Fig. 8 presents the first cited ratio for the two categories, which has been analysed here as IC/TL. This change is required because in some cases CG flashes are null and the ratio losses its sense. In both cases, IC flashes dominate throughout the 13 min, with a predominance of normalized values of 0.9–1.0 for the ratio in both groups. However, G1 shows a higher variability of the ratio. In particular, the P50 fluctuates between 0.96 and 0.98 in mid-period, descending in the last minutes. Therefore, CG flashes increase at some moments during the 13 min, mainly in the last 2 min before the LJW is triggered. On the contrary, G2 shows a more constant trend (P50 fluctuating between 0.96 and 0.97), with a smooth increase of IC flash number during the first six minutes after which it remains constant.

Regarding the $+CG/-CG$ ratio, the absence of positive strokes in some periods has led to calculating this relationship in another way, that is using instead the ratio $-CG$ over the total CG strokes. Results for

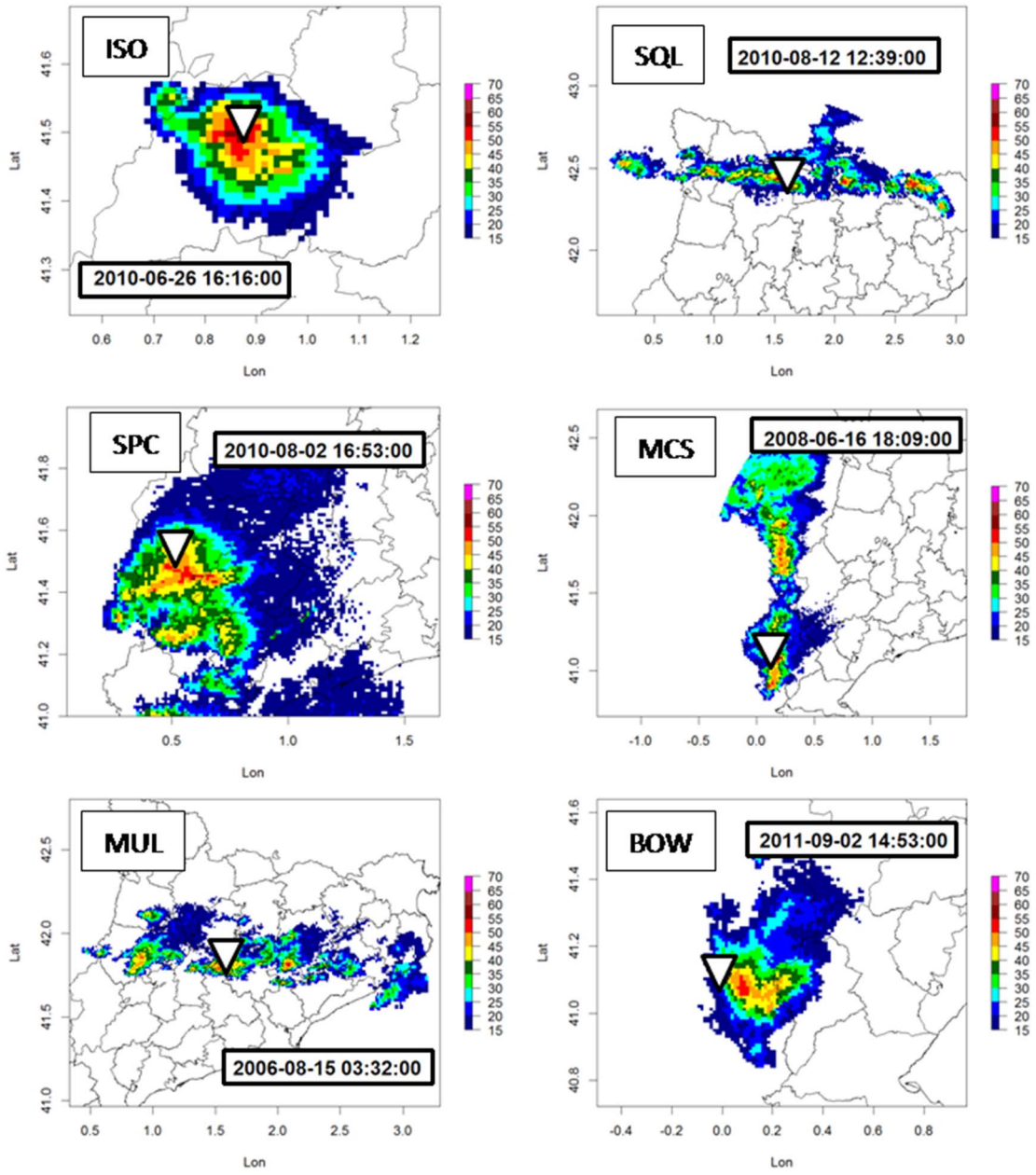

Fig. 4. Classification of radar structures in the study. The white triangles are the LJW and the coloured contour areas depict the reflectivity fields associated with the thunderstorms that produced the LJW. Longitude and latitude units are in degrees.

this ratio (Fig. 9) present moderate differences between the two groups. G1 (< 2 cm) group shows more remarkable fluctuations during the period than G2. The $-$CG flashes dominate throughout all the period. The P50 shows an increasing trend from minutes 7 to 13. This means that during these 6 min, $+$CG flash rate increases with respect to $-$CG. G2 also shows a significant dominance of $-$CG throughout all the period with a more important presence of $+$CG than in the G1 case. The evolution of the ratio for this latter group is similar to the evolution for G2, with sudden rises of $+$CG in specific moments, leading to positive anomalies ($+$CG $>$ $-$CG).

4.4. Evolution of each type of lightning

Following with the analysis of the influence of each type of flashes (IC, $-$CG and $+$CG), TL and Area, the evolution of each of these variables during the 13 min before the LJW has been examined. The purpose of this study is to determine whether an increase in the activity of the different variables occurs for all types of flashes. This work has been carried on according to the division explained in step 4 of Section 3.5 (see Fig. 10).

The first issue is that TL and IC flashes do not register big differences between the three flash types, which can be explained considering that the contribution of IC to TL is higher than 95%. However, the negative trend slightly dominates in both groups. Otherwise, Area, $-$CG and $+$CG flashes show a neutral trend.

The predominance of IC during the 13 min period for all type of hail events (see the previous section), is understandable considering its higher importance when the LJW is triggered. Hence, the most common situation is an increase of flashes just before the alert. Before this increase, nevertheless, the trend of the flash number is variable. Therefore, the evolution of flashes before the minute 12 is not indicative of a future triggering of a LJW. Moreover, no remarkable differences between the two thunderstorm groups have been found, following a similar trend in both cases.

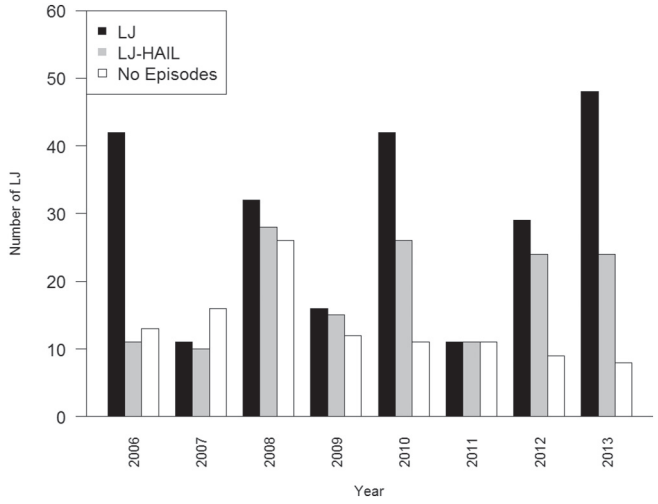

Fig. 5. Time evolution of total LJW (black bars), LJW related to hail episodes (grey bars) and number of hailstorms per year (white bars).

4.5. Lead time and distance between LJ and observations

The lead time has shown promising results for the analysed events. The median value for the set of the cases is 55 min, meaning that the triggering of the LJW occurs, in average, near one hour before the observation of hail at surface (see Fig. 11, left panel). Moreover, most of the cases have presented a LT between 20 and 100 min.

Considering the LT by groups (see Fig. 11, right panel), the differences between G1 and G2 are few. The median is close to 55 min in both, while the interquartile range is of 17 to 101 min for G1, and of 19 to 98 min for G2.

Regarding the distance between the LJW position (that is, the centroid of the flashes' cell at the time when the algorithm triggers the alert) and the maximum number of observations recorded by the hailpads, the median is approximately 60 km. For the bulk of cases, this distance lies between 35 and 100 km (Fig. 12, left panel). This means that thunderstorms had a long trajectory from the triggering of the LJW to the observation of hail at the surface.

Fig. 12 (right panel) shows more significant differences between groups than for the case of the LT. In the case of G1, the distance between LJW and the maximum at the surface shows a larger distance between the warning position and the observation of hail. For this group, the median is located at 75 km and the interquantile range is of 46 to 112 km. On the contrary, G2 shows a more grouped structure. The median is located at 51 km, whereas the interquartile range is of 27 to 76 km. Considering these results and taking into account both the LWJ parameter and the LT, the G1 thunderstorms moved with higher speed. The speed of the cells could have also been estimated by means of weather radar imagery, but this calculation is more complicated because in some cases the structures present a high degree of complexity.

4.6. Evolution of the vertical profile of reflectivity

In this sense, the reflectivity profiles (for the P25, median, P75 and P99 areas) are rather different between categories, as Fig. 13 shows. It is important to recall that only 1-10 km layer has been studied, because of the configuration of the volumetric radar product used in the analysis. This radar task was configured in this way because of two reasons: the necessity of a quick and easy to work product, and also because 10 km is the average top height of most thunderstorms (considering a 12 dBZ reflectivity threshold) analysed in the region, although higher values are possible. Moreover, the properties of the levels over this threshold do not provide relevant information to the forecasters.

G1. The evolution of the reflectivity at high levels in the thunderstorms of G1 (< 2 cm) shows a funnel shape pattern. Starting from a minimum of reflectivity at lower levels, this variable presents an increase until the 5 km level. At higher altitudes, the reflectivity decreases (see Fig. 13, left panel).

G2. Reflectivity shows in most of cases an increase from 1 km to 4 km, followed by a moderate rise until around 7 km. At the top of the profile, the curve remains practically constant for the first part of the sample (P25 and P50) whereas the reflectivity decreases for the other part (P75 and P99). This profile presents a bow-like shape (see Fig. 13, center panel).

4.7. Radar structures

The radar mode of the structures related to LJW have been studied in order to determine if a predominance of any of the types presented in the methodology is observed. It is important to recall that the analysis has been done considering only the radar image that is closest in time to the LJ warning. According to the classification explained in Section 3.5, the SQL structure is the most frequent in the episodes studied with 35.6%, followed by the SPC structure type, with 31.8%. Both types of structure usually present long life-cycles and strong updrafts. The rest of the LJ are distributed as follows: 13.6% of the sample contains a MCS structure and 12.9% belong to MUL structure. The less frequent structures are BOW and ISO constituting only a 4.5% and 1.5% of the sample (not shown).

Regarding the classification of structures by groups, there is a similar distribution between the two groups considered. The small number of episodes with MUL structure found in G1 is remarkable, however(see Fig. 14).

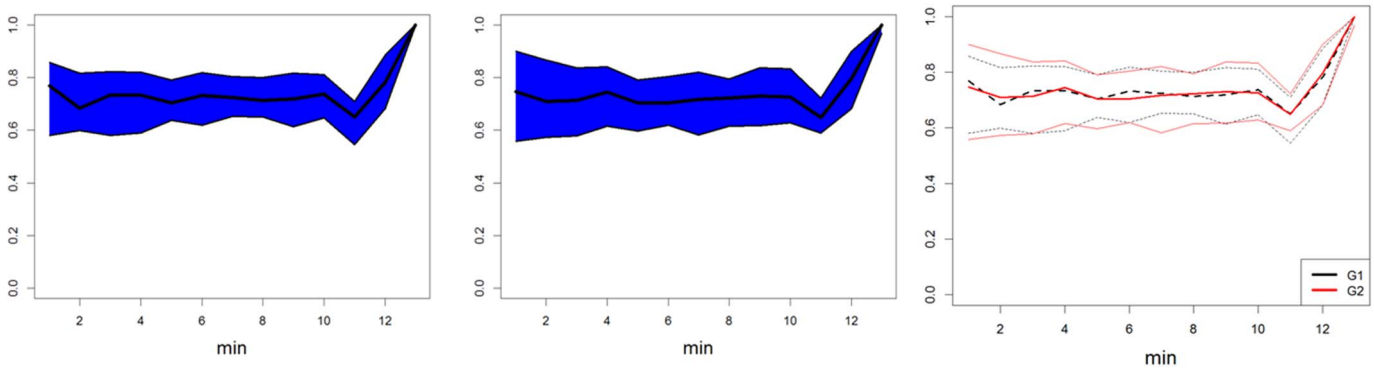

Fig. 6. Evolution of the normalized Total Lightning (TL) variable throughout the 13 min previous to the LJ: left) G1 -small hail size-; centre) G2 -large hail size-; right) Comparison between G1 and G2. Legend of left and centre panels: the bold line indicates the median and shadowed area represents the interval between P25 and P75.

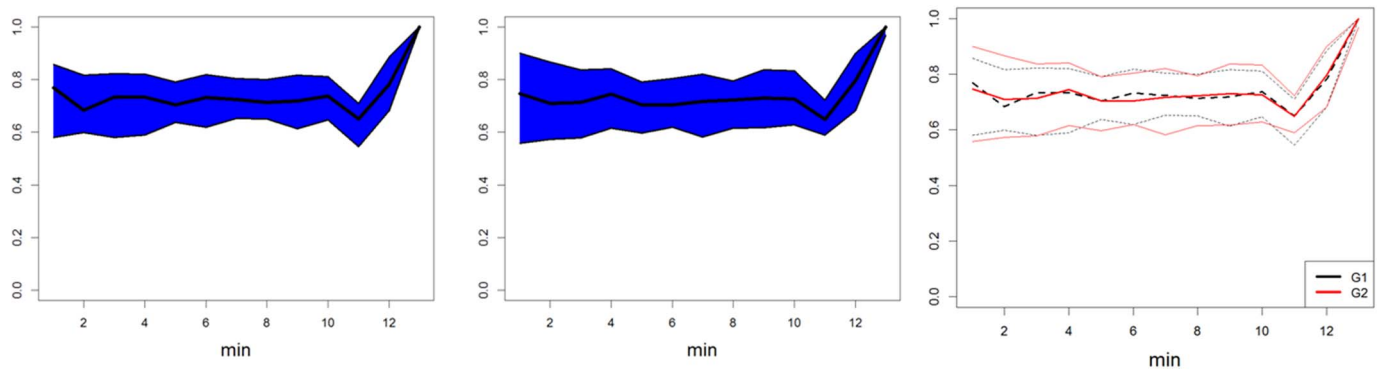

Fig. 7. As in Fig. 6 but for the Area variable.

5. Discussion

The preliminary analysis has shown that most hailstorms in Catalonia take place between April and September, a period similar to that in other countries (Saltikoff et al., 2010; Wapler, 2017). According to Aran et al. (2011), the most common synoptic patterns related to hailstorms in Lleida are " Short wave through"(SWT) and "Ireland Low"(IL). Both patterns are associated with low depressions located at the west of the studied area. This fact would explain why the most affected zone by hailstorms is the western part, as shown in Section 4. This is caused by thunderstorms that are developed in the Ebro Valley and move to the area pushed by easterly or north-easterly flows.

Moving to the TL characteristics prior to the LJW, large rates of this variable, around or more than 50 flashes per minute are required. The thunderstorms with a large TL are explained by the strong vertical updrafts. These updrafts allow a strong development of the cloud, with an increased growth and collision rate between particles (Deierling and Petersen, 2008). In this sense, the formation of a stratiform region where the distant flashes are generated is also possible (Pédeboy et al., 2016). The thunderstorms showing a high TL are also related to a larger area, in most of cases. While in isolated thunderstorms or in multicellular systems the area is limited, in supercell thunderstorms or quasi linear convective systems, the extent can reach larger values. These hypotheses agree strongly with our results, because in most of the LJW cases, the thunderstorm presented a supercellular or squall line mode. Considering the evolution of the normalized values of the TL and the area, similar behaviours have been observed for both groups. Therefore, it is complicated to forecast hail size considering the evolution of these variables.

Moreover, IC flashes dominate over CG flashes in all groups, presenting values above 0.9. That is, more than 90% of the flashes in thunderstorms are ICs. The predominance of ICs support the findings of Schultz et al. (2011), who showed that it is difficult to predict severe weather using only CG data. In this sense, the same authors analyzed the lightning algorithm taking only into account CG and missed a significant portion (46%) of severe weather events in supercellular thunderstorms. Besides, from a simple analysis using the F2017 algorithm, but without ICs flashes, the results indicate that the warnings were reduced to the 1%, failing in most of the main severe weather cases. Other authors observed the predominance of IC flashes according to the phase of the thunderstorm. For instance, Montanyà et al. (2009) observed a large IC rate prior to severe convective weather, followed by a decrease of the lightning activity during the hail shaft. These observations agree with our results, because this analysis is focused on the phase of the thunderstorm prior to the severe weather occurrence. Similar results can be found in Montanyà et al. (2007) or MacGorman et al. (1989).

In the analysis of CG flashes, a dominance of −CG in all groups has been observed. Nevertheless, in G1 and G2 increases of +CG have been detected in some periods prior to the LJ occurrence. Montanyà et al. (2009) observed a high IC flash rate while +CG were dominant in some phases of storms life cycle. Several studies (e.g. Carey and Rutledge, 1998; Soula et al., 2004; Wiens et al., 2005) suggest that the thunderstorms associated to severe weather can have a predominance of +CG during the mature phase of thunderstorm. However, severe weather can also take place without a predominance of +CG (e.g. Carey and Rutledge, 2003; Williams, 2001). Despite in some cases of study positive anomalies have been observed, as shown in the results, a wide range of different behaviours have been recorded. Hence, this is not a regular pattern to be used as hail-size forecaster.

Until now, several authors have studied the evolution of the flashes for the period during which hail is recorded. In the case of +CG flashes, the majority of strokes are taking place when the hail is falling on the ground. Wapler (2017) found that the stroke rate increases before the observations of hail and decreases afterwards.

The LT is an important characteristic of the LJ because it measures the time available to warn population about severe weather. This parameter has been calculated in some studies (Goodman et al., 2005;

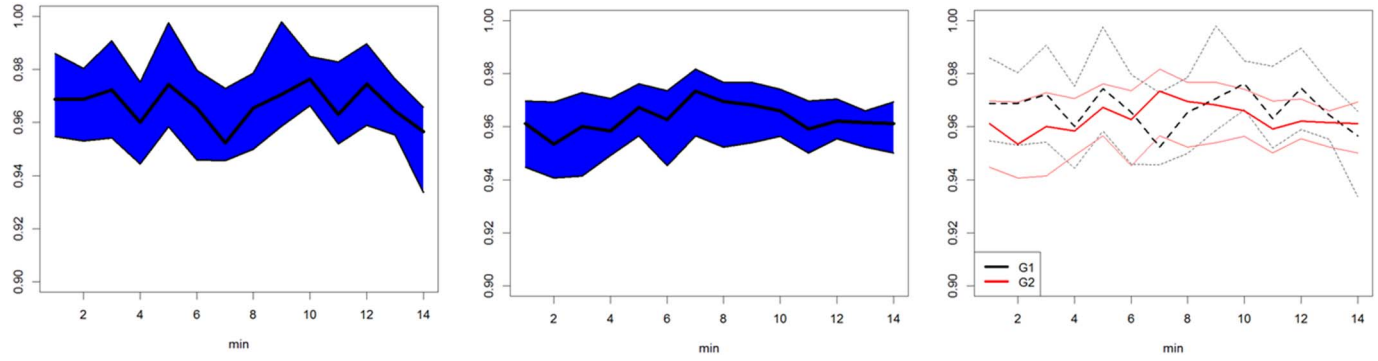

Fig. 8. As in Fig. 6 but for the normalized relation between IC flashes and TL.

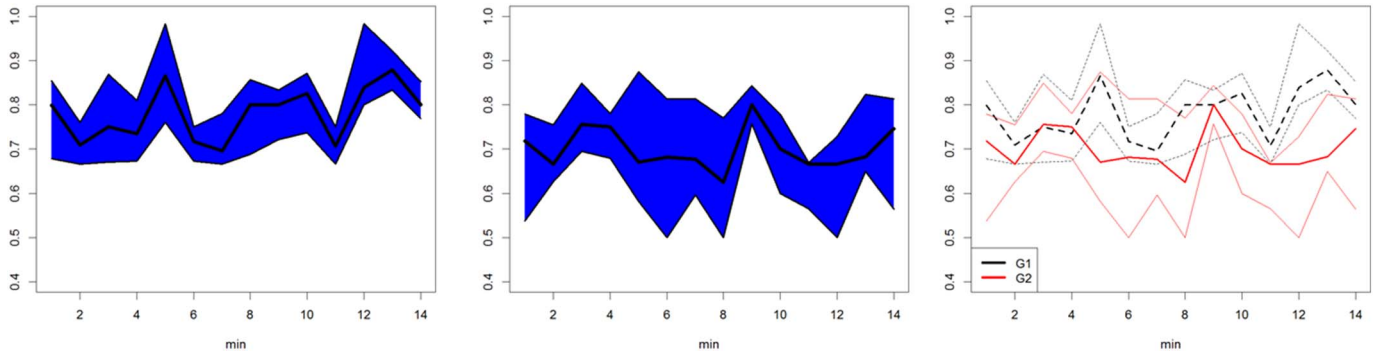

Fig. 9. As in Fig. 6 but for the relation between -CG flashes and Total CG flashes.

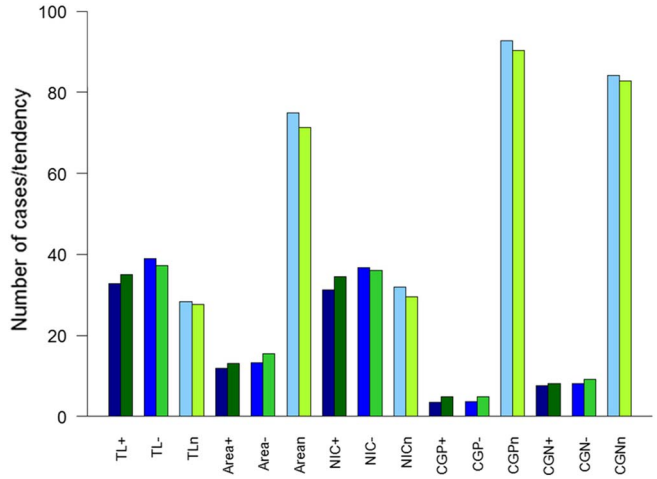

Fig. 10. Trend of different variables during the previous minutes to LJ. Blue and green colours refer to G1 and G2 thunderstorms, respectively.

Steiger et al., 2007; Williams et al., 1999), which have obtained a LT of around 5 and 30 min. The LT calculated in the present study has been higher than their results, because the time interval is wider and ranges between 17 and 100 min(for the most number of cases). The LT by groups does not show important differences, both groups with median values of around 55 min. The LT does not show an important difference between the two groups, both with a median (Q2, P50) of around 55 min.

In regard to the distance between the LJW position and the observations recorded by hailpads, this parameter shows a median of around 60 km and the interquartile range is of 35 to 100 km. Moreover, some differences between groups have been detected. For instance, the LJWs of G1 are associated to a higher distance between the warning and the observation with a median of 75 km. On the contrary, G2 presents lower distances than G1 with a median of 51 km and the interquartile range of 26 to 76 km. These results are very valuable in terms of short-term forecast and surveillance, because they provide a measure of how far the severe weather is shifted with respect to the coordinates where the alert is triggered.

In addition to linking the LT with radar parameters, it must be pointed out that at the time of LJW occurrence, thunderstorms with hail size > 2 cm (G2) have a lower vertical development than those which produced hail of a size under 2 cm (G1). Therefore, it is probable that these characteristics had changed at the time of the hailshaft, because most of the G2 thunderstorms are still in a less developed stage when the LJW is recorded. This results coincide and would explain why the extension of the area for G1 is higher than for G2. In any case, although the structures can change their mode throughout the life cycle, the real fact is that the change can always be related with the degree of organization. In this sense, it seems complicated that poorly organized structures (isolated or multi-cell) could easily reach a high degree of organization. Thus, squall-lines and super-cell structures are strongly related with a higher number of LJW and also a larger hail size.

Regarding the vertical profiles of reflectivity, Zipser and Lutz (1994) studied vertical profiles related to severe weather of different regions of the world. The profiles obtained in mid-latitude continental and tropical continental regions are similar to the G2 profiles in the current study. According to Williams (2001), the vertical profiles of reflectivity with higher values at mid and high levels correspond to strong updrafts, associated with high vertical speeds Browning et al. (1976). This implies that hail size can be larger (Van Den Heever and Cotton, 2004) than in other cells with moderate updrafts. In any case, as pointed out by Nelson (1983), the updraft strength is not an exclusive factor, and the buoyant factor must also be taken into account, which helps the growth of the hailstones inside the thunderstorm. In fact, these previous observations can be linked with the profile observed for G2, which contains higher values of reflectivity at mid and high levels

As pointed out before, those structures associated with a high degree of convection (SQL and SPC) are more prone of producing a LJW than other structures (ISO and MUL). This point is connected with the second paragraph of the present section, which makes reference to the TL rates. It is important to have in mind that the cases of MCS and BOW should be considered apart, because it is possible that SQL changes to

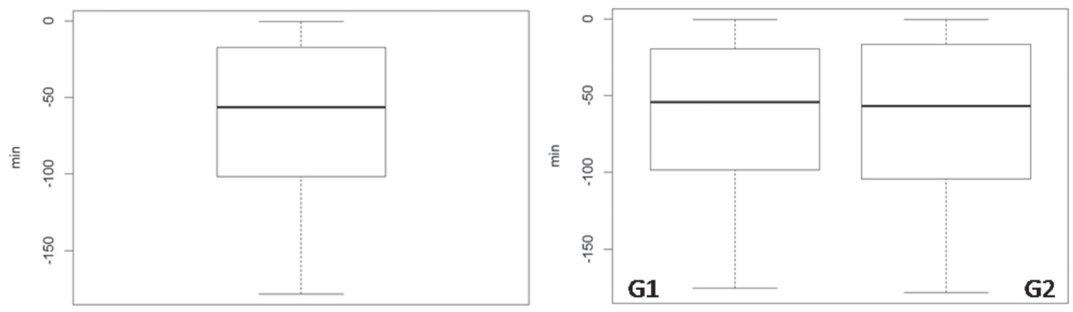

Fig. 11. Lead time between the LJW and the observation at the surface: a) for all cases and b) by groups.

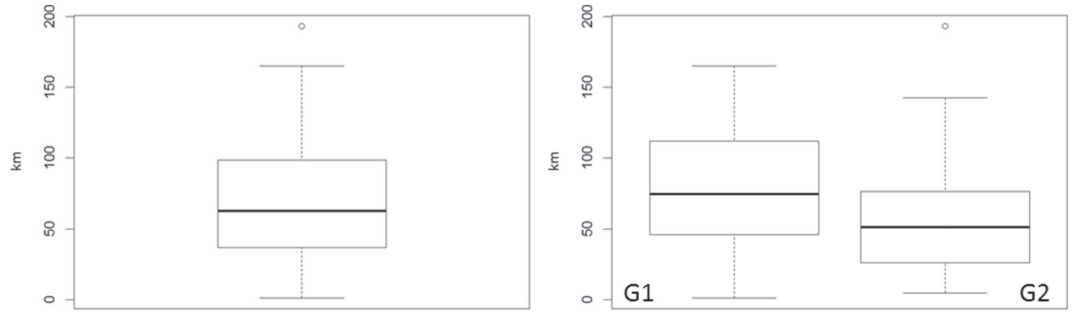

Fig. 12. a) Distance between the LJ and the observation for each LJ. b) Distance between the LJ and the observation according to the groups.

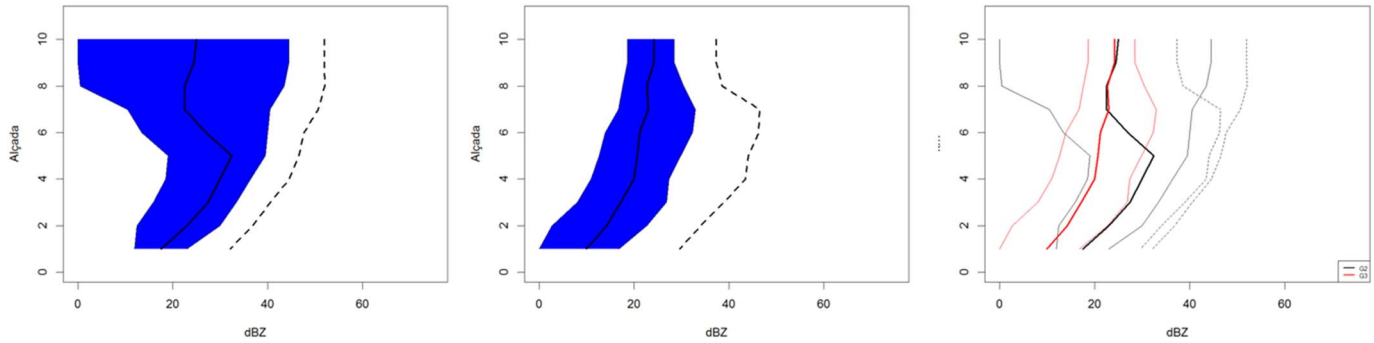

Fig. 13. Same as Fig. 6 but for reflectivity vertical profiles. The black dashed lines in left and central figures represent P99.

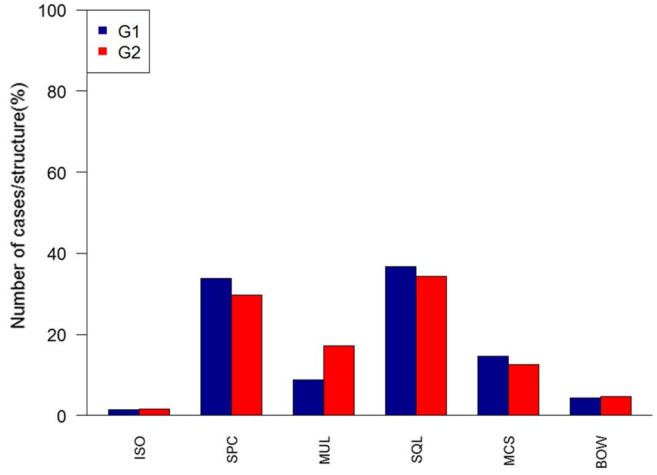

Fig. 14. Classification of radar structures related to LJ.

those structures during the life cycle. In any case, the analysis only considers the time at which the LJ warning was triggered and a lack of cases of those modes of convection has been observed. Finally, addressing the relationship between LJW and the degree of organization, it was observed that alerts are not only observed in more cases for those well-organised structures, but also that when a structure of the type SPC or SQL is observed, the probability of triggering more than one warning in a short period is high. In other words, it is quite frequent that a SPC or SQL structure for which a warning is issued, triggers more warnings during its whole life cycle. On the contrary, ISO and MUL cases only present one warning throughout the complete life span of the structure. This aspect is related with the fact that updrafts in well-organized structures tend to be stronger than in other structures, helping to increase the charge layers' gap.

An analysis carried on in this paper has studied the differences between two groups. This study initially included an additional group: little hail (< 2 cm), medium hail (2–4 cm) and big hail (> 4 cm). The last group presented remarkable differences compared to the other two groups but the sample was too small to be representative. For this reason, it was finally considered reasonable to reduce the analysis to 2 groups, considering 2 cm as the threshold (which is commonly considered for severe hail). Anyway, several differences with the extreme values of G2 can be observed in the results.

6. Conclusions

This study initially presents a brief climatology of hailstorms in the Lleida Plain region during the studied period (2006–2013). However, the main point of the manuscript has been the analysis of several lightning and radar parameters related to LJW. The thunderstorms have been divided in two groups, according to hail size, in order to observe flow behaviours for each group. Also, the type of lightning has been considered in part of the analysis.

The western part of the area was the most affected by the hailstorms that produced at least one LJ warning. 75% of thunderstorms affected a small number of hailpads. For this reason, it is difficult to associate the number of affected hailpads with the size of thunderstorms. Throughout most of the year, the number of LWJs is higher than the number of hail episodes. Hence, in each hail episode one or more LWJs may be recorded. However, no clear relationship between the maximum hail diameter of hail and the number of LJW could be observed. In an interannual evolution analysis for the studied period, the number of hailstorm episodes/year and the maximum size of hail/year did not coincide, showing the high variability of this type of phenomenon.

Answering the question of what type of flashes dominates during the 13 min previous to LJ alerts, IC flashes dominate without variations to the over CG. Regarding the CG portion, there is a dominance of $-$CG over $+$CG. Nevertheless, sudden increases of $+$CG in some parts of the studied period have been observed in both groups.

Considering the evolution of TL and area during these 13 min, the evolutions were similar in the two groups with small variations during the first 10 min and a slight decrease in minute 11, followed by a strong increase between minutes 12 and 13. The only difference between both groups is found in area, G1 showing higher values than G2. Therefore,

the total lightning number and the extension of the area can be used to estimate the magnitude of the thunderstorms.

Analysing the trend during the 13 min(without considering the last 2 min) according to the type of flashes, TL and Area for each group, a slight dominance is found of the negative trend in TL and IC flashes, and a neutral trend in Area, −CG and +CG.

Taking into account the LT and the distance between LJW and observations at surface, in most of the cases the LJW triggers within one and half hour and 20 min before the hail impacts are recorded, according to the whole set of cases. In the analysis by groups, LT does not show a remarkable difference between the two groups. The pattern observed is a median located at 55 min and a interquartile of 20 to 100 min.

With regard to the distance between the LJW and the observations recorded by hailpads, it presents a median around 60 km and an interquartile of 35 (Q1) to 100 km (Q3). Some differences between groups have been found. The LJ alerts associated with G1 correspond to a larger distance between the warning and the observation. On the contrary, G2 presents a structure very similar to that of the LT, with less dispersion in the set of values. In this case, the maximum value is lower than for G1.

In relation to the analysis of the behaviour of several radar variables at the time of the LJW, important differences between the thunderstorms of G1 and G2 groups have been found. The main ones correspond to the reflectivity profile. The percentiles of each group show different evolutions in the different levels analysed. G1's profile presents a funnel shape and the G2's profile presents a bow shape. This can also be used as a forecaster of the hail size.

Finally, those structures associated with a high degree of convection (SQL and SPC) are more prone to produce a LJ than other structures (ISO). Regarding the relationship between LJW and the degree of organization, it is observed that LJ not only take place in more cases for those well-organised structures, but also that when a structure of the type SPC or SQL is observed, the probability of issuing more than one warning in a short period is high.

Even though the LJ algorithm provides very valuable information for hail nowcasting, with very good values of lead time and distance, clear difficulties for providing a short-time forecast of the hail size have been found. Probably, the cause is that the warnings in thunderstorms with small hail are triggered in a later stage of the life cycle. Hence, the features of most of the variables are similar to those of the thunderstorms producing larger hail. For this reason, the authors recommend the combined use of radar and lightning data in order to determine the phase of the thunderstorm at the time of the LJW.

Acknowledgements

The authors wish to thank Patricia Altube for her very valuable comments, the Associacio de Defensa Vegetal (ADV-Pla de Lleida), the Grupo de Fisica de la Atmosfera, from the University of Leon, and the Research Area of the Servei Meteorologic de Catalunya (SMC) for the data.

References

Aran, M., Pena, J., 2009. Atmospheric circulation patterns associated with hail events in lleida (catalonia), preprints. In: 5th European Conference on Severe Storms. ECSS.
Aran, M., Pena, J.C., Torà, M., 2011. Atmospheric circulation patterns associated with hail events in Lleida (Catalonia). Atmos. Res. 100 (4), 428–438.
Boudevillain, B., Andrieu, H., 2003. Assessment of vertically integrated liquid (VIL) water content radar measurement. J. Atmos. Oceanic Technol. 20 (6), 807–819.
Bringi, V., Vivekanandan, J., Tuttle, J., 1986. Multiparameter radar measurements in Colorado convective storms. Part II: Hail detection studies. J. Atmos. Sci. 43 (22), 2564–2577.
Browning, K., Foote, G., 1976. Airflow and hail growth in supercell storms and some implications for hail suppression. Quart. J. Roy. Meteor. Soc. 102 (433), 499–533.
Browning, K., Frankhauser, J., Chalon, J.-P., Eccles, P., Strauch, R., Merrem, F., Musil, D., May, E., Sand, W., 1976. Structure of an evolving hailstorm part v: synthesis and implications for hail growth and hail suppression. Mon. Wea. Rev. 104 (5), 603–610.
Carey, L.D., Rutledge, S.A., 1998. Electrical and multiparameter radar observations of a severe hailstorm. J. Geophys. Res.: Atmospheres 103 (D12), 13979–14000.
Carey, L.D., Rutledge, S.A., 2003. Characteristics of cloud-to-ground lightning in severe and nonsevere storms over the central United States from 1989–1998. J. Geophys. Res.: Atmospheres 108 (D15).
Castro, A., Sánchez, J., Fraile, R., 1992. Statistical comparison of the properties of thunderstorms in different areas around the Ebro-valley (Spain). Atmos. Res. 28 (3), 237–257.
Dalezios, N.R., Loukas, A., Bampzelis, D., 2002. Universal kriging of hail impact energy in greece. Phys. Chem. Earth A/B/C 27 (23), 1039–1043.
Deierling, W., Petersen, W.A., 2008. Total lightning activity as an indicator of updraft characteristics. J. Geophys. Res.: Atmospheres 113 (D16).
Dessens, J., 1986. Hail in southwestern France. I: hailfall characteristics and hailstrom environment. J. Appl. Meteor. Climatol. 25 (1), 35–47.
Doswell III, C.A., 2001. Severe convective storms-an overview. In: Severe Convective Storms. Springer, pp. 1–26.
Edwards, R., Thompson, R.L., 1998. Nationwide comparisons of hail size with WSR-88d vertically integrated liquid water and derived thermodynamic sounding data. Weather Forecast. 13 (2), 277–285.
Farnell, C., Busto, M., Aran, M., Andres, A., Pineda, N., Torà, M., 2009. Study of the september 17th 2007 severe hailstorm in pla d'urgell. Part I: fieldwork and analysis of the hailpads. Tethys: J. Mediterranean Meteorol. Climatol. 6, 69–81.
Farnell, C., Rigo, T., Martin-Vide, J., 2016. Application of cokriging techniques for the estimation of hail size. Theor. Appl. Climatol. 1–19.
Farnell, C., Rigo, T., Pineda, N., 2017. Lightning jump as a nowcast predictor: application to severe weather events in catalonia. Atmos. Res. 183, 130–141.
Fraile, R., Castro, A., Sánchez, J.L., Marcos, J.L., López, L., 2001. Noteworthy c-band radar parameters of storms on hail days in northwestern Spain. Atmos. Res. 59, 41–61.
Gatlin, P.N., Goodman, S.J., 2010. A total lightning trending algorithm to identify severe thunderstorms. J. Atmos. Oceanic Technol. 27 (1), 3–22.
Giaiotti, D., Nordio, S., Stel, F., 2003. The climatology of hail in the plain of Friuli venezia giulia. Atmos. Res. 67, 247–259.
Goodman, S.J., Blakeslee, R., Christian, H., Koshak, W., Bailey, J., Hall, J., McCaul, E., Buechler, D., Darden, C., Burks, J., et al., 2005. The north Alabama lightning mapping array: recent severe storm observations and future prospects. Atmos. Res. 76 (1), 423–437.
Goodman, S.J., Buechler, D.E., Wright, P.D., Rust, W.D., 1988. Lightning and precipitation history of a microburst-producing storm. Geophys. Res. Lett. 15 (11), 1185–1188.
Heinselman, P.L., Priegnitz, D.L., Manross, K.L., Smith, T.M., Adams, R.W., 2008. Rapid sampling of severe storms by the national weather radar testbed phased array radar. Weather Forecast. 23 (5), 808–824.
Kitzmiller, D.H., McGovern, W.E., Saffle, R.F., 1995. The WSR-88d severe weather potential algorithm. Weather Forecast. 10 (1), 141–159.
Krauss, T.W., Marwitz, J.D., 1984. Precipitation processes within an Alberta supercell hailstorm. J. Atmos. Sci. 41 (6), 1025–1035.
Krauss, T.W., Renick, J., 1997. The new Alberta hail suppression project. J. Wea. Mod. 29 (1), 100–105.
Lang, T.J., Rutledge, S.A., Dye, J.E., Venticinque, M., Laroche, P., Defer, E., 2000. Anomalously low negative cloud-to-ground lightning flash rates in intense convective storms observed during STERAO-a. Mon. Wea. Rev. 128 (1), 160–173.
MacGorman, D.R., Burgess, D.W., Mazur, V., Rust, W.D., Taylor, W.L., Johnson, B.C., 1989. Lightning rates relative to tornadic storm evolution on 22 May 1981. J. Atmos. Sci. 46 (2), 221–251.
Makitov, V., 1999. Organization and main results of the hail suppression program in the northern area of the province of Mendoza, Argentina. J. Wea. Mod. 31 (1), 76–86.
Makitov, V.S., Inyukhin, V.S., Kalov, H.M., Kalov, R.H., 2016. Radar research of hailstorm formation and development over the central part of northern Caucasus (Russia). Organization and main results of the regional hail suppression projects. Nat. Hazards Rev. 1–20.
Metzger, E.L., 2010. The relationship between total cloud lightning behavior and radar derived thunderstorm structure. In: Tech. rep. DTIC Document.
Montanyà, J., Pineda, N., March, V., Illa, A., Romero, D., Solà, G., 2006. Experimental evaluation of the Catalan lightning detection network. In: 19th International Lightning Detection Conference, Tucson.
Montanyà, J., Soula, S., Pineda, N., 2007. A study of the total lightning activity in two hailstorms. J. Geophys. Res.: Atmospheres 112 (D13).
Montanyà, J., Soula, S., Pineda, N., van der Velde, O., Clapers, P., Solà, G., Bech, J., Romero, D., 2009. Study of the total lightning activity in a hailstorm. Atmos. Res. 91 (2), 430–437.
Montanyà, J., Van der Velde, O., March, V., Romero, D., Solà, G., Pineda, N., 2012. High-speed video of lightning and x-ray pulses during the 2009–2010 observation campaigns in northeastern Spain. Atmos. Res. 117, 91–98.
Nelson, S.P., 1983. The influence of storm flow structure on hail growth. J. Atmos. Sci. 40 (8), 1965–1983.
Palencia, C., Berthet, C., Massot, M., Castro, A., Dessens, J., Fraile, R., 2007. On the individual calibration of hailpads. Atmos. Res. 83 (2), 493–504.
Pascual, R., 2002. Estudio de las granizadas en el llano de Lleida. Nota técnica(3).
Pédeboy, S., Barnéoud, P., Berthet, C., 2016. First results on severe storms prediction based on the French national lightning locating system. In: 24th International Lightning Detection Conference and 6th International Lightning Meteorology Conference. Vaisala, Vaisala April.
Pineda, N., Montanyà, J., 2009. Lightning detection in Spain: the particular case of catalonia. In: Lightning: Principles, Instruments and Applications. Springer, pp. 161–185.

Pineda, N., Rigo, T., Montanà, J., Van der Velde, O., 2016. Charge structure analysis of a severe hailstorm with predominantly positive cloud-to-ground lightning. Atmos. Res. 178, 31–44.
Przybylinski, R.W., 1995. The bow echo: Observations, numerical simulations, and severe weather detection methods. Weather Forecast. 10 (2), 203–218.
Punge, H., Kunz, M., 2016. Hail observations and hailstorm characteristics in Europe: a review. Atmos. Res. 176, 159–184.
Rigo, T., Llasat, M., 2004. A methodology for the classification of convective structures using meteorological radar: Application to heavy rainfall events on the Mediterranean coast of the Iberian peninsula. Nat. Hazards Earth Syst. Sci. 4 (1), 59–68.
Rigo, T., Llasat, M.C., 2016. Forecasting hailfall using parameters for convective cells identified by radar. Atmos. Res. 169, 366–376.
Rigo, T., Pineda, N., 2016. Inferring the severity of a multicell thunderstorm evolving to supercell, by means of radar and total lightning. Electronic J. Severe Storms Meteor. 11 (2).
Rigo, T., Pineda, N., Bech, J., 2010. Analysis of warm season thunderstorms using an object-oriented tracking method based on radar and total lightning data. Nat. Hazards Earth Syst. Sci. 10 (9), 1881–1893.
Saltikoff, E., Tuovinen, J.-P., Kotro, J., Kuitunen, T., Hohti, H., 2010. A climatological comparison of radar and ground observations of hail in Finland. J. Appl. Meteor. Climatol. 49 (1), 101–114.
Sánchez, J., Fraile, R., De La Madrid, J., De La Fuente, M., Rodríguez, P., Castro, A., 1996. Crop damage: the hail size factor. J. Appl. Meteor. 35 (9), 1535–1541.
Schultz, C.J., Carey, L.D., Schultz, E.V., Blakeslee, R.J., Goodman, S.J., 2014. Physical and dynamical linkages between lightning jumps and storm conceptual models. In: XV International Conference on Atmospheric Electricity, 15-20 June 2014, Norman, Oklahoma, U.S.A..
Schultz, C.J., Petersen, W.A., Carey, L.D., 2009. Preliminary development and evaluation of lightning jump algorithms for the real-time detection of severe weather. J. Appl. Meteor. Climatol. 48 (12), 2543–2563.
Schultz, C.J., Petersen, W.A., Carey, L.D., 2011. Lightning and severe weather: a comparison between total and cloud-to-ground lightning trends. Weather Forecast. 26 (5), 744–755.
Smith, B.T., Thompson, R.L., Grams, J.S., Broyles, C., Brooks, H.E., 2012. Convective modes for significant severe thunderstorms in the contiguous United States. Part I: storm classification and climatology. Weather Forecast. 27 (5), 1114–1135.
Soula, S., Seity, Y., Feral, L., Sauvageot, H., 2004. Cloud-to-ground lightning activity in hail-bearing storms. J. Geophys. Res.: Atmospheres 109 (D2).
Steiger, S.M., Orville, R.E., Carey, L.D., 2007. Total lightning signatures of thunderstorm intensity over north Texas. Part I: Supercells. Mon. Wea. Rev. 135 (10), 3281–3302.
Trapero, L., Bech, J., Rigo, T., Pineda, N., Forcadell, D., 2009. Uncertainty of precipitation estimates in convective events by the meteorological service of Catalonia radar network. Atmos. Res. 93 (1), 408–418.
Trapp, R.J., Wheatley, D.M., Atkins, N.T., Przybylinski, R.W., Wolf, R., 2006. Buyer beware: some words of caution on the use of severe wind reports in postevent assessment and research. Weather Forecast. 21 (3), 408–415.
Tuovinen, J.-P., Punkka, A.-J., Rauhala, J., Hohti, H., Schultz, D.M., 2009. Climatology of severe hail in Finland: 1930–2006. Mon. Wea. Rev. 137 (7), 2238–2249.
Van Den Heever, S.C., Cotton, W.R., 2004. The impact of hail size on simulated supercell storms. J. Atmos. Sci. 61 (13), 1596–1609.
Wapler, K., 2017. The life-cycle of hailstorms: lightning, radar reflectivity and rotation characteristics. Atmos. Res. 193, 60–72.
Wiens, K.C., Rutledge, S.A., Tessendorf, S.A., 2005. The 29 June 2000 supercell observed during STEPS. Part II: lightning and charge structure. J. Atmos. Sci. 62 (12), 4151–4177.
Williams, E., Boldi, B., Matlin, A., Weber, M., Hodanish, S., Sharp, D., Goodman, S., Raghavan, R., Buechler, D., 1999. The behavior of total lightning activity in severe Florida thunderstorms. Atmos. Res. 51 (3), 245–265.
Williams, E., Weber, M., Orville, R., 1989. The relationship between lightning type and convective state of thunderclouds. J. Geophys. Res.: Atmospheres 94 (D11), 13213–13220.
Williams, E.R., 2001. The electrification of severe storms. In: Severe Convective Storms. Springer, pp. 527–561.
Witt, A., Eilts, M.D., Stumpf, G.J., Johnson, J., Mitchell, E.D.W., Thomas, K.W., 1998. An enhanced hail detection algorithm for the WSR-88d. Weather Forecast. 13 (2), 286–303.
Yao, W., Zhang, Y., Meng, Q., Wang, F., Lu, W., 2013. A comparison of the characteristics of total and cloud-to-ground lightning activities in hailstorms. Acta Meteorol. Sin. 27, 282–293.
Zipser, E.J., Lutz, K.R., 1994. The vertical profile of radar reflectivity of convective cells: a strong indicator of storm intensity and lightning probability? Mon. Wea. Rev. 122 (8), 1751–1759.